Science of the Total Environment 752 (2021) 141829

Contents lists available at ScienceDirect

Science of the Total Environment

journal homepage: www.elsevier.com/locate/scitotenv

Conversion mechanisms between organic sulfur and inorganic sulfur in surface sediments in coastal rivers

Ming Jiang [a,b], Yanqing Sheng [a,*], Qunqun Liu [a,b], Wenjing Wang [a], Xiaozhu Liu [a,b]

[a] Research Center for Coastal Environment Engineering Technology of Shandong Province, Yantai Institute of Coastal Zone Research, Chinese Academy of Sciences, Yantai, China
[b] University of Chinese Academy of Sciences, Beijing, China

HIGHLIGHTS

- Environmental transformation of RIS and OS in coastal rivers was identified.
- OS formation was attributed to sedimentary environments of Fe and OM availability.
- RIS sedimentation was controlled by the ES and reactive Fe oxides.
- Terrigenous inputs and sulfurization enhanced FAS release.
- Autochthonous biological inputs facilitated HAS immobilization.

GRAPHICAL ABSTRACT

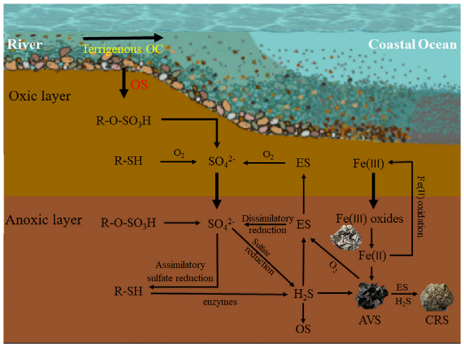

ARTICLE INFO

Article history:
Received 19 June 2020
Received in revised form 1 August 2020
Accepted 18 August 2020
Available online 20 August 2020

Editor: Filip M.G. Tack

Keywords:
Coastal rivers
Sediment
Inorganic sulfur
Organic sulfur
Buffer capacity

ABSTRACT

Geochemical processes of sulfur (S) in river aquatic systems play a crucial role in environmental evolution. In this study, the distributions and sources of reduced inorganic sulfur (RIS) and organic sulfur (OS) in coastal river surface sediments were investigated. The results indicated that OS dominated total S (80%), and OS (*i.e.*, humic acid sulfur, HAS; fulvic acid sulfur, FAS) correlated with the availability of labile organic matter (OM) and reactive iron (Fe). Terrigenous inputs and sulfurization contributed to the enrichment of FAS through the S reduction. Autochthonous biological inputs were potential sources of HAS from S oxidization. The X-ray photoelectron spectroscopy showed that the main sources of S in surface sediments were deposited as the form of organic ester-sulfate. Aquatic life could break S down further, producing reduced S compounds accumulated as thiols and RIS in anoxic sediments. RIS was dominated by acid volatile sulfur (AVS) and chromium (II)-reducible sulfur (CRS). Reactive Fe oxides were major control factors for the conversation from hydrogen sulfide (H_2S) to AVS, whereas elemental sulfide (ES) controlled the conversion from AVS into CRS in coastal rivers.

1. Introduction

Sulfur (S) plays an important role in the diagenesis and preservation of organic matter (OM) in sediments (Ma et al., 2019). River sediments are important repositories and sinks for S (Qin et al., 2019). The geochemical process of the S cycle in aquatic system exists in a large variety of organic and inorganic forms (Wang et al., 2016). Different S fraction conversion in sediments may influence environmental evolution and ecological safety (Oueslati et al., 2018; Jørgensen et al., 2019).

Coastal rivers can be characterized as regions surrounded by areas of excess nutrients and high pollutant loads with active sulfate reduction (Qin et al., 2019; Liu et al., 2020). Generally, contaminant deposition may stimulate benthic mineralization and oxygen depletion in surface

* Corresponding author.
E-mail address: yqsheng@yic.ac.cn (Y. Sheng).

https://doi.org/10.1016/j.scitotenv.2020.141829
0048-9697/

sediments, and sulfate becomes the dominant terminal electron acceptor to oxidize OM, promoting dissimilatory sulfate reduction (Sun et al., 2016; Ma et al., 2019). Dissolved hydrogen sulfide (HS^- and H_2S) produced during dissimilatory sulfate reduction may quickly react *via* several ways depending on environmental conditions (Wang et al., 2012; Wang et al., 2016). There are three main pathways: oxidation by chemical and biological processes, formation of reduced inorganic sulfur (RIS), and formation of organic sulfur (OS) (Riedinger et al., 2017; Fakhraee and Katsev, 2019). Oxidation is prominent within oxic-anoxic interfaces (*e.g.*, sediment resuspension and flocculation) where sulfide encounters oxidants, such as oxygen and oxidized metal ion species (*e.g.*, MnO_2, Eq. (1)) (van de Velde et al., 2018; Zhang et al., 2018). This oxidation converts H_2S back to sulfate and forms reduced S intermediates (*e.g.*, polysulfides) (Giuffrè and Vicente, 2018; Zhang et al., 2020), acting as precursors for the formation of RIS and OS (Eq. (2)). In the presence of reactive Fe, the reduced S may be reacted to acid volatile sulfide (AVS) (Eq. (3)) and eventually chromium (II)-reducible sulfur (CRS) (Eq. (4)) (Sun et al., 2016). AVS and CRS are two major end products of RIS in coastal sediments (Kraal et al., 2013; Sheng et al., 2015; Sun et al., 2016). The transformation from AVS to CRS is typically controlled by the OM, reactivity of Fe minerals and the availability of dissolved sulfate buried in sediments (Morgan et al., 2012; Yang et al., 2020), which can be identified by the AVS/CRS ratios, the degree of pyritization (DOP) and sulfurization (DOS).

$$H_2S + MnO_2 \rightarrow S^0 + Mn^{2+} \quad (1)$$

$$O_2 + H_2S \rightarrow S^0, SO_4^{2-}, SO_3^{2-}, S_2O_3^{2-} + H_2O \quad (2)$$

$$H_2S + Fe^{2+} \rightarrow FeS + 2H^+ \quad (3)$$

$$FeS + H_2S \rightarrow FeS_2 + H_2 \quad (4)$$

Additionally, sulfide can be sequestered as OS during OM sulfurization and assimilatory sulfate reduction, producing humic S in surface sediments (Chen et al., 2014; Fakhraee et al., 2017). This OS can be further divided into humic acid S (HAS) and fulvic acid S (FAS) (Brüchert, 1998). Active incorporation of reduced S intermediates into HAS and FAS has been observed in estuary salt marshes (Ferdelman et al., 1991; Brüchert, 1998), groundwater systems (Einsiedl et al., 2008), eutrophic bay (Zhu et al., 2013) and marine mud sediments (Zhu et al., 2014). Coastal water polluted by excess inputs of nutrients from terrestrial sources or salt-water intrusion may enhance the accretion of OM mineralization and trapping of inorganic sediments (Nasir et al., 2016; Riedinger et al., 2017). As a result of transformations, sulfide production and oxidation cause rapid deoxygenation and acidification of the overlying water during sediment resuspension (Morgan et al., 2012; Wang et al., 2020). Under this circumstance, free sulfide may accumulate in porewater, posing detrimental effects on benthic ecosystems if it cannot be effectively buffered by sedimentary Fe oxides (Sheng et al., 2015; Shi et al., 2019). Therefore, the enhancement of buffering capacity (0.5 mol/L HCl extractable Fe, the Fe pool most readily to buffer dissolved sulfide over short-time scales) is particularly important to assess the health status of benthic ecosystem and its resilience for rapid environmental changes. (Zhu et al., 2012; Liu et al., 2014).

Previous studies about S geochemical process mainly focused on diagenetic interactions among RIS in marine sediments (Zhu et al., 2013; van de Velde et al., 2018; Qin et al., 2019). However, the conversion mechanisms between RIS and OS in sediments are unclear, especially in coastal rivers with stresses of terrestrial pollution and high salinity brine inputs. The objectives of this study were to (1) investigate the spatial distributions of S in the surface sediments in different types of coastal rivers, (2) quantify the buffering capacity of sedimentary Fe against sulfides in coastal rivers, and (3) identify the anthropogenic impacts on S—Fe mineral accumulation and transformation in coastal river sediments.

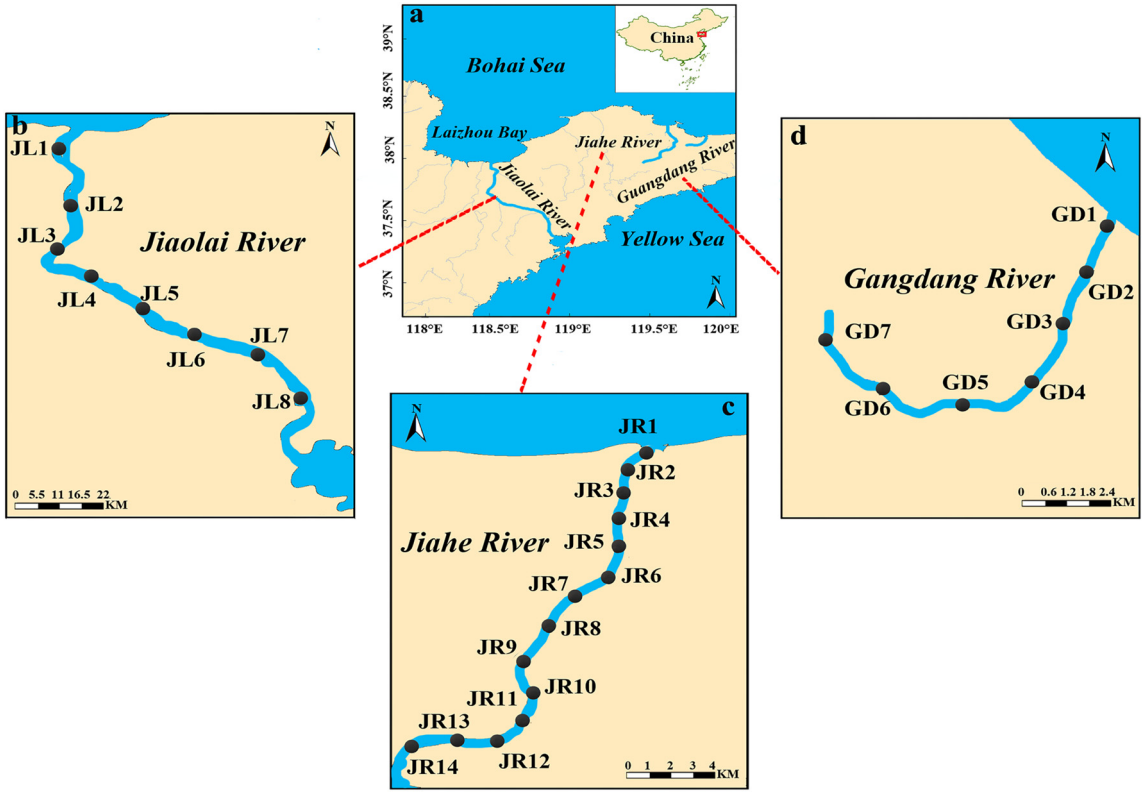

Fig. 1. Sampling locations in study area (a, overall map; b, JL; c, JR; d, GD).

2. Material and methods

2.1. Study area description and sampling

Jiaolai River (JL), Jiahe River (JR) and Guangdang River (GD) are three typical coastal rivers in the Shandong Peninsula, China (Fig. 1). The length of the JL is approximately 130 km with a watershed area of 5478.6 km^2. This river is of great importance given its vast flux into the Bohai Sea, and it provides irrigation and industrial water over a catchment of 3900 km^2 (Zhao et al., 2019). Many potential industrial effluents (salt fields) and non-point source agricultural pollution are noted along the JL. The sediments in JL bear a long-term exposure with bitter brine discharge salt fields and potential pollutant inputs from industries. The JR stretches for approximately 140 km, and the total watershed area spans 2296 km^2. JR is the source of drinking water as it is located away from industrial areas and has less anthropogenic perturbations, entering the north Yellow sea (Liu et al., 2020). The watershed area of JR is 1224 km^2, originating from the Menlou reservoir (largest reservoir in the local city). A series of rubber dams have been constructed in the main stream to provide drinking water and prevent seawater invasion. As a drinking water source, the sediments in JR nearly can be regarded as undefiled sediment. The GD is a municipal flood discharge river, and it flows into the North Yellow Sea with a total length of 8 km. The GD is an artificial urban river with high chemical oxygen demand (50 mg/L, Li et al., 2016), which is mainly affected by domestic sewage and few potential industrial effluents. To provide a water landscape, the riverbed of GD was constructed using concrete many years ago instead of natural sediments. Many low concrete dams were also constructed to maintain the GD river water levels. Therefore, as an artificial urban river, the sediments in GD is shallow (<20 cm), and there is no permeation in riverine bottom.

Sediment samples were collected from different rivers (Fig. 1). Surface sediments were collected using a stainless steel grab sampler. Immediately, samples were stored in sealed plastic bags filled with N_2 in an icebox and were transported to the laboratory within 8 h. All samples were frozen at −18 °C until further handling. Dissolved oxygen (DO), pH, electrical conductivity (EC), salinity and oxidation-reduction potentials (ORP) were measured using a YSI Professional Plus handheld multiparameter instrument (YSI Incorporated, Yellow Springs, USA). Water samples (obtained approximately 20 cm under the surface water) from each site were collected synchronously using a water sampler.

2.2. Carbon, nitrogen and grain size analysis

The samples were homogenized and vacuum freeze dried, then were grinded and sieved through a size 100 mesh for further analysis. For total organic carbon (TOC) determination, sample was acidified with 1 mol/L HCl for 16 h to remove carbonates. Subsequently, the mixture was washed using Milli-Q water to remove HCl and was then lyophilized for TOC analysis. For total nitrogen (TN) determination, the sample was not subject to hydrochloric acid treatment. TOC and TN in sediments were determined using a TOC-V_{CPH}/SSM-5000A (Shimadzu, Japan, RSD ≤ 3%) analyzer. The mass ratio of TOC to TN was displayed as C/N. The particle sizes of sediments were analyzed using a laser particle size analyzer (Mastersizer 2000F, Malvern, UK, RSD < 2.5%). The percentages of the following three groups of grain sizes were determined: <4 μm (clay), 4–63 μm (silt), and >63 μm (sand).

2.3. S fraction extraction

Generally, the RIS in fresh sediments were operationally defined as AVS (sulfides extracted by hydrochloric acid, primarily FeS), CRS (primarily pyritic sulfur), and elemental sulfur (ES, a combination of oxidation products) (Berner et al., 1970). Briefly, AVS (6 mol/L HCl, 1 h), CRS (15 mL acidic Cr(II), 2 h) and ES (5 mL Cr(II) + 20 mL *N*,*N*-dimethylformamide + 5 mL concentrated HCl, 1 h) using a sequential fractionation procedure (Sheng et al., 2015). Pure N_2 was used as carrier gas to purge and trap hydrogen sulfide (H_2S) at 60 ± 1 °C (by electric hot plate). Sulfide was released as H_2S during AVS, CRS and ES extraction. H_2S was trapped as CuS in $CuCl_2$ (0.1 mol/L) traps. Here, 0.5 and 1 mg/L sulfide solutions (Na_2S) were used in the recovery experiments (average sulfide recovery rate was 96%). The measured sulfide data were converted to real sulfide content after correction for the recovery rate. The precision of triplicate analyses was generally less than 5% for each fraction.

The OS fraction extraction for FAS and HAS was based on the reported method (Zhu et al., 2013). Briefly, approximately 5 g wet sample was sequentially washed with 0.5 mol/L NaCl and 1 mol/L HCl under N_2 atmosphere and acetone to remove sulfate, AVS and ES, respectively. The residual sample was extracted with 0.1 mol/L NaOH (15 mL) under N_2 for 24 h to extract humic substances. The extraction procedure was repeated (5 to 8 times) until the extract was faintly yellow. The supernatants were separated by centrifugation (4000*g*, 20 min), and the filtrates were acidified to pH 2 to precipitate humic acid over 48 h. The supernatant was collected for FAS analysis, and the precipitate was separated by centrifugation for HAS determination. The precipitate was freeze-dried, ground, and calcined at 800 °C for 2 h to convert HAS to sulfate following Eschka's procedure (Mott and Wilkinson, 2007). The resultant sulfate was dissolved in Milli-Q water (60 °C, 30 min) prior to filtration. The extracted solution was acidified to pH 2, and then excess 10% (*w*/*v*) $BaCl_2$ (10 mL) was added to precipitate sulfate as $BaSO_4$ and weighed by gravimetry. For FAS, 20 mL H_2O_2 (30% *v*/v) was added to the supernatant at 60 °C for 1 h. The H_2O_2 oxidation procedure was repeated thrice to ensure complete oxidation of FAS to sulfate. The sulfate was precipitated as $BaSO_4$ and weighted for FAS calculation.

2.4. Solid phase Fe extraction

The speciation of solid-phase Fe was divided into total labile Fe (LFe, including LFe(II) and LFe(III)), total reactive Fe (RFe, including RFe(II), RFe(III)) and sodium dithionite extractable Fe (FeD). LFe is designated as biologically reactive Fe, and LFe(III) is mainly obtained from amorphous and poorly crystalline Fe(III)-oxyhydroxides (Azzoni et al., 2005). LFe(II) mainly consists of Fe sulfides (pyrite excluded). RFe is designated as the fraction of Fe in sediments that readily reacts with sulfide to form various Fe sulfide minerals and eventually pyrite (Canfield, 1989). FeD is mainly composed of Fe oxides and oxyhydroxides (Zhu et al., 2012). Briefly, approximately 1 g wet sample was extracted with 0.5 mol/L HCl (25 mL, 12 h), 6 M HCl (25 mL, 12 h), and 50 g/L sodium dithionite (25 mL, 12 h) successively and then centrifuged (3000*g*, 15 min). Supernatants were filtrated for Fe(II) (LFe(II) and RFe(II)), LFe and RFe determination. LFe, RFe and FeD concentrations in the extracts were measured using the 1,10-phenanthroline method (Kraal et al., 2013). Both LFe(II) and RFe(II) were measured by the same method but without hydroxylamine. Dissolution and reduction of the entire quantity of Fe(III) (LFe(III) and RFe(III)) were ensured by spiking with 1 mL HCl (1:1) and 1 mL 10% (wt%) hydroxylamine hydrochloride. LFe(III) and RFe(III) were the difference between LFe and LFe(II) and between RFe and RFe(II), respectively. The repeated measurement error was less than 8%.

2.5. Sulfate in porewater and X-ray photoelectron spectroscopy (XPS) analysis

Porewater was extracted by centrifugation at 4000*g* for 20 min and filtered through 0.45 μm. The filtrate (porewater) was diluted approximately 15 times for sulfate analysis *via* barium chromate spectrophotometry (HJ/T 342-2007, Chinese standard) and determined by a UV–visible spectrophotometer (UV-2450, Shimadzu Co., Tokyo, Japan) at 420 nm. Powdered samples were pressed onto indium foil with a clean spatula for XPS analysis. XPS spectra were obtained on the American

ThermoFischer ESCALAB 250Xi spectrometer using Al Ka excitation (hv = 1486.6 eV). The monochromatic Al X-ray source was operated at low power (14.6 kV, 13.5 mA). The emitted photoelectrons were detected by the analyzer with a passing energy of 20 eV and 0.1-eV steps.

2.6. Data calculation

Chemical buffer capacity (β_L) is a measure of the actual buffer capacity of rapid buffering towards dissolved sulfide and is described in equation (Eq. (5)) based on that reported by Azzoni et al. (2005) as follows:

$$\beta_L = [\mathrm{LFe(II)} - \mathrm{AVS}] + 1.5 \times \mathrm{LFe(III)} \quad (5)$$

$$3S^{2-} + 2\mathrm{Fe(III)} = S^0 + 2\mathrm{FeS} \quad (6)$$

where [LFe(II) - AVS] is the buffering capacity of Fe(II) that has not yet been sulfurized, and 1.5 LFe(III) is the buffering capacity of labile Fe (III) oxides that quickly buffer dissolved sulfide according to the 3:2 stoichiometry between S^{2-} and FeS (3:2) in Eq. (6) (Zhu et al., 2012).

The degree of pyritization (DOP) and sulfurization (DOS) can be used to characterize pyritization and sulfurization of reactive Fe availability relevant to quick buffering of dissolved sulfide and is calculated by Eqs. (7) and (8) (Berner et al., 1970) as follows:

$$\mathrm{DOP} = \mathrm{Fe\ (CRS)}/[\mathrm{Fe\ (CRS)} + \mathrm{Fe\ (HCl)}] \quad (7)$$

$$\mathrm{DOS} = [\mathrm{Fe\ (AVS)} + \mathrm{Fe\ (CRS)}]/[\mathrm{Fe\ (CRS)} + \mathrm{Fe\ (HCl)}] \quad (8)$$

where Fe (CRS) is the amount of Fe bound to CRS, which is calculated by CRS/2 according to the 1:2 stoichiometry of FeS_2; Fe (AVS) is sulfide-bound Fe(II) assuming that AVS predominantly occurs as FeS; and Fe (HCl) is the "residual" reactive Fe that has not been pyritized. The availability of highly reactive Fe relevant to quick buffering of dissolved sulfide in sediments was quantified by FeD to characterize pyritization and sulfurization.

3. Results

3.1. Properties of overlying water and sediments

General parameters of overlying water are shown in Table S1. The pH values in JL, JR and GD ranged from 2.79 to 8.28, 6.42 to 8.61, and 8.03 to 8.85, respectively. The salinity in JL (mean 6.41 ± 0.01 PSU) was increased compared with JR (0.47 ± 0.01 PSU) and GD (0.50 ± 0.01 PSU) except for the estuaries. Both DO and ORP values in three rivers were greater than 6.4 mg/L and 117 mV, respectively. The average Ec in JR (6.8 ± 0.02 ms/cm) was lower than that in JL (17.9 ± 0.01 ms/cm) and GD (19.2 ± 0.01 ms/cm). Higher coefficients of variation of Ec and salinity were observed in JR (2.1 and 2.3, respectively), indicating increased variation of these parameters along the river compared to JL (1.1 and 1.3, respectively) and GD (1.2 and 1.2, respectively). As shown in Fig. 2, sand dominated the sediment particle size in JL (77 ± 0.03%), JR (65 ± 0.02%) and GD (58 ± 0.03%), indicating the effects of rainwater erosion and transport. The highest sedimentary TOC and TN were noted in GD with average values of 2.62 ± 0.01% and 0.27 ± 0.01% respectively, followed by JR (1.17 ± 0.01% and 0.17 ± 0.01%) and JL (0.25 ± 0.01% and 0.04 ± 0.01%). Overall, TOC and TN in coastal rivers exhibited a decreasing trend from upstream to estuary expect for GD. The C/N ratios (TOC/TN) of sediments are displayed in Table S2. The mean C/N ratio was 8.5 ± 0.30 in JL, which was close to JR (8.4 ± 0.13) but lower than that in GD (10.5 ± 0.12). Sulfate concentrations in porewater ranged from 1210.50 ± 28.07 to 7782.02 ± 38.23 mg/L in JL (mean 5562.25 ± 47.33 mg/L), 63.21 ± 9.61 to 2333 ± 74.86 mg/L in JR (mean 490 ± 22.54 mg/L) and 51.31 ± 19.22 to 2337.30 ± 72.09 mg/L in GD (mean 716 ± 34.33 mg/L), respectively (Fig. 3).

3.2. Distributions of different Fe species

The distribution of different Fe species is illustrated in Fig. 4. The LFe average in GD was 93.82 ± 2.08 μmol/g, which was increased compared with that noted in JL (54.64 ± 2.36 μmol/g) and JR (60.17 ± 2.54 μmol/g). In all rivers, the averages of LFe(III) (6.72 ± 0.32, 17.31 ± 1.76 and 14.57 ± 0.46 μmol/g in JL, JR and GD respectively) were far lower than LFe(II) (47.92 ± 2.11, 42.86 ± 1.27 and 79.25 ± 1.64 μmol/g, respectively). These results indicated that LFe(II) dominated the LFe, and a large portion of LFe(III) was reduced. However, the average total RFe in JR (182.80 ± 10.62 μmol/g) and GD (190.92 ± 13.48 μmol/g) were increased compared with that noted in JL (143.22 ± 14.44 μmol/g), with RFe(III) averages of 154.28 ± 7.96, 144.5 ± 9.83 and 107.28 ± 5.66 μmol/g, in JR, GD and JL, respectively. These values were considerably increased compared with RFe(II) values at all sites (28.52 ± 2.66, 46.44 ± 3.64 and 35.94 ± 8.78 μmol/g in JR, GD and JL, respectively). The RFe(III) content was considerably increased compared with LFe(III), exhibiting a similar variation trend to RFe along the rivers. Overall, RFe(III) dominated the RFe in these coastal rivers. A large portion of RFe (III) remained unreduced, or RFe(II) was oxidized. Averaged FeD values in JL, JR and GD were 19.08 ± 2.05, 25.38 ± 2.21 and 30.18 ± 3.00 μmol/g, respectively (Fig. 4).

3.3. AVS/CRS, DOP and DOS variations

In this study, AVS/CRS ratio (Table S2) varied from 0.34 to 4.78 in JL (mean 2.29 ± 0.17), 0.01 to 2.89 in JR (mean 0.78 ± 0.19) and 0.12 to 1.86 in GD (mean 1.18 ± 0.08). The average DOP and DOS values were 0.13 ± 0.02 and 0.68 ± 0.05 in JL, 0.31 ± 0.03 and 0.61 ± 0.08 in JR, 0.39 ± 0.03 and 1.34 ± 0.13 in GD, respectively. Overall, the highest AVS/CRS value was noted for JL, while the highest DOP and DOS values were observed for GD.

3.4. Distribution of S fractions

The spatial distribution of S fractions in surface sediments is illustrated in Fig. 5 and Table S3. OS (sum of HAS and FAS) accounted for 89%, 85% and 77% of total S in JL, JR and GD, respectively (Fig. 5a). FAS was the dominant component of OS in JL (76%) and GD (75%) with average values of 234.89 ± 11.01 and 241.61 ± 13.16 μmol/g, respectively, whereas HAS dominated OS in JR (74%) at 161.68 ± 7.98 μmol/g (Fig. 5b). HAS in JL and GD exhibited narrow average values of 37.98 ± 2.60 μmol/g and 79.09 ± 6.35 μmol/g, respectively, which were considerably lower than that in JR.

RIS (sum of AVS, CRS and ES) in GD sediments were 4-fold and 3-fold increased compared with JL and JR, respectively. The average AVS contents in JL (17.08 ± 0.69 μmol/g) and GD (60.11 ± 3.88 μmol/g) were increased compared with JR (10.48 ± 1.94 μmol/g). In JL and GD, AVS was the main component of RIS (65% and 70% of RIS in JL and GD, respectively), exhibiting a consistent spatial trend in the upper reach with unusually high values at JL6 (1000.62 ± 13.66 μmol/g) and GD3 (392.16 ± 29.80 μmol/g). However, CRS dominated RIS (70%) in JR with an average of value was of 25.10 ± 1.38 μmol/g, which was increased compared with JL (6.71 ± 0.68 μmol/g) but less than the GD (42.90 ± 1.64 μmol/g). The ES shared the lowest proportion of RIS in JL, JR and GD at 1.4%, 0.03% and 1.7% of RIS, respectively. ES content exhibited a consistent reducing trend from upstream to downstream in JL, JR and GD with averaged contents of 2.51 ± 0.25, 0.09 ± 0.02 and 6.87 ± 0.51 μmol/g, respectively.

3.5. XPS results

Three representative sediment samples (JL6, JR10, GD3) were selected for XPS determination. The site selection for these three sites were based on their sediment environmental characteristics, mainly including contents of sulfate, OS (FAS and HAS), RIS (AVS, CRS and ES), different

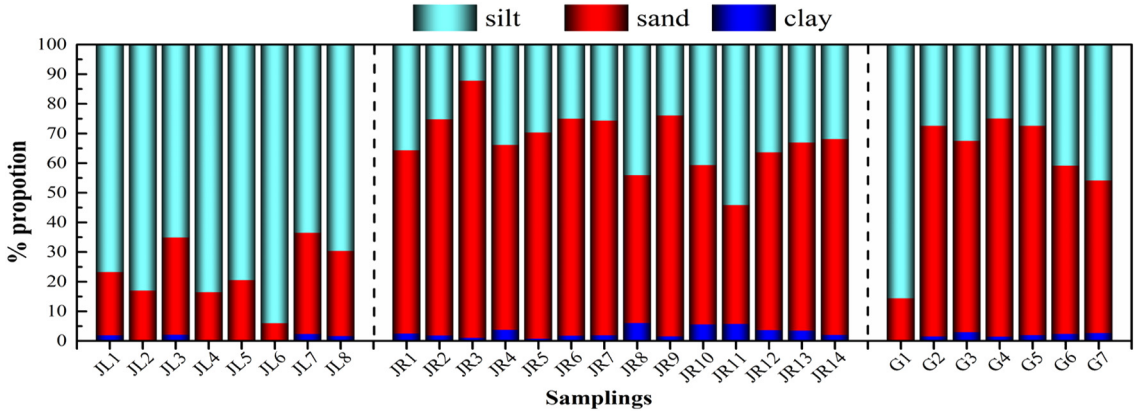

Fig. 2. Spatial distribution of grain size composition of surface sediments.

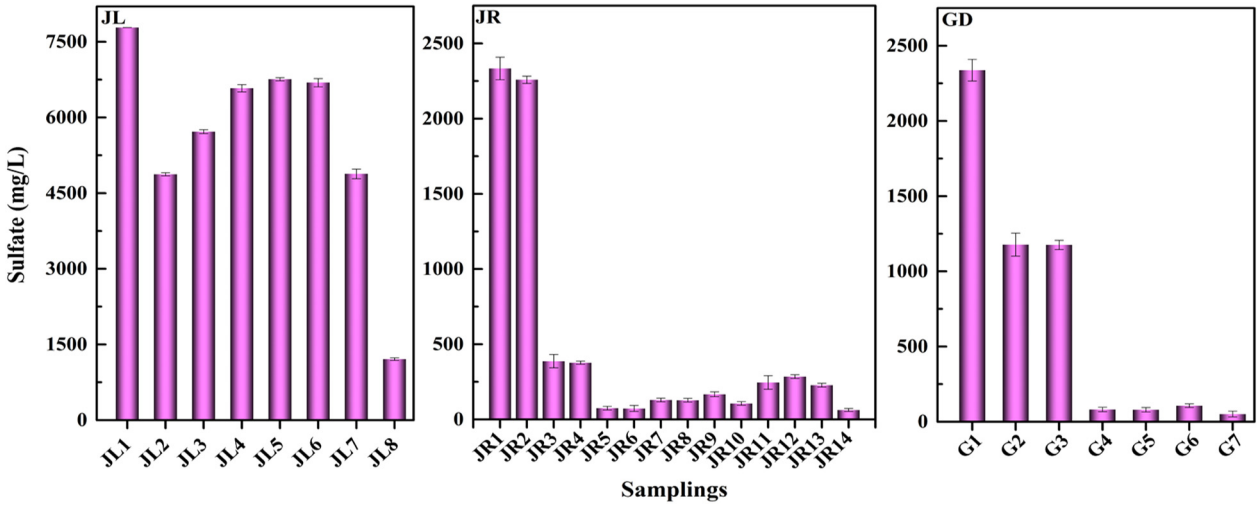

Fig. 3. Concentrations of sulfate in porewaters in different coastal rivers.

Fe fractions and the potential pollution source along the river. The XPS fitting curves of C1s and S2p levels and analysis results of S speciation were presented in Fig. 6 and Table 1, respectively. The C1s spectrum revealed sharp peaks at 284.0-eV binding energy with a low tail towards higher binding energies. This observation suggested the existence of variable functional groups (particularly, oxidized carbons, *e.g.*, O=C=O, C—O, C=O) in three rivers. The spectral simulation of S2p photopeaks at high binding energies (167.4–169.1 eV) corresponded to highly oxidized S (+4 to +6), including sulfate, sulfate esters, sulfones and sulfonates (Fakhraee et al., 2017). This component was detected in all specimens with the highest abundance of 33–67% of the total amount of S. Photopeaks at low binding energies (163.5–164.7 eV) were attributed to OS entities, which were close to reduced S (−2 to +2) (Couture et al., 2016). Corresponding organic species may include thiols, thiophenes and disulfides. Their content in sediments ranged from 17 to 33% of the total amount of S.

4. Discussion

4.1. Source discriminations of depositional OM in sediments

The C/N ratio is frequently used to identify historical sources of sedimentary OM and indicates the watersheds influenced by human disturbance (Nasir et al., 2016). When sedimentary OM primarily originates from endogenous materials (*e.g.*, algae) containing abundant aquatic protein-rich and cellulose-poor organisms, it typically has a C/N ratio between 6 and 10. When the C/N ratio is greater than 15, sedimentary OM is mainly derived from terrestrial plants that are protein in poor and cellulose rich (Meyers, 1997). In this work, high C/N ratios were observed in several sites in JL (JL1, 15.08 ± 0.25; JL6, 14.22 ± 0.21) and most sites in GD (most sites >10, except GD1), which were close to the range for typical terrestrial sources. This result indicated that external inputs already significantly impacted JL and GD. High TOC values were primarily observed in the upper and lower reaches of JL and the middle reach of GD where it flowed through urban areas (including some special industrial parks). Thus, water quality was potentially affected by the inputs of pollutants from industrial and living sources, yielding acidic pH (low as 2.79 ± 0.03) and alkalescence pH (up to 8.85 ± 0.01) values in JL and GD, respectively. Moreover, a low ratio in most sites of JL is attributed to frequent artificial disturbance of sediments, such as dredging and sand excavation, resulting in low OM deposition (Liu et al., 2020). However, this ratio was ranged from 4 and 12 in JR, which was close to the range for aquatic algae, suggesting that internal phytoplankton contributes to OM in JR. The hydraulic conditions have been changed drastically by the series of rubber dams (Bao et al., 2020), and the slow water current contributed to an increased proportion of fine particles (clay) with high TOC deposition in the middle reach of JR (Fig. 2 and Table S1). The dammed urban river typically suffers from blooms of macrophyte and phytoplankton alternatively (Bao et al., 2020). The decomposition of settled phytoplankton debris contributed to the sinking of algae OM particulate into surface sediments (Yang et al., 2011; Wang et al., 2012). Thus, the process of humification or mineralization in aquatic environments can

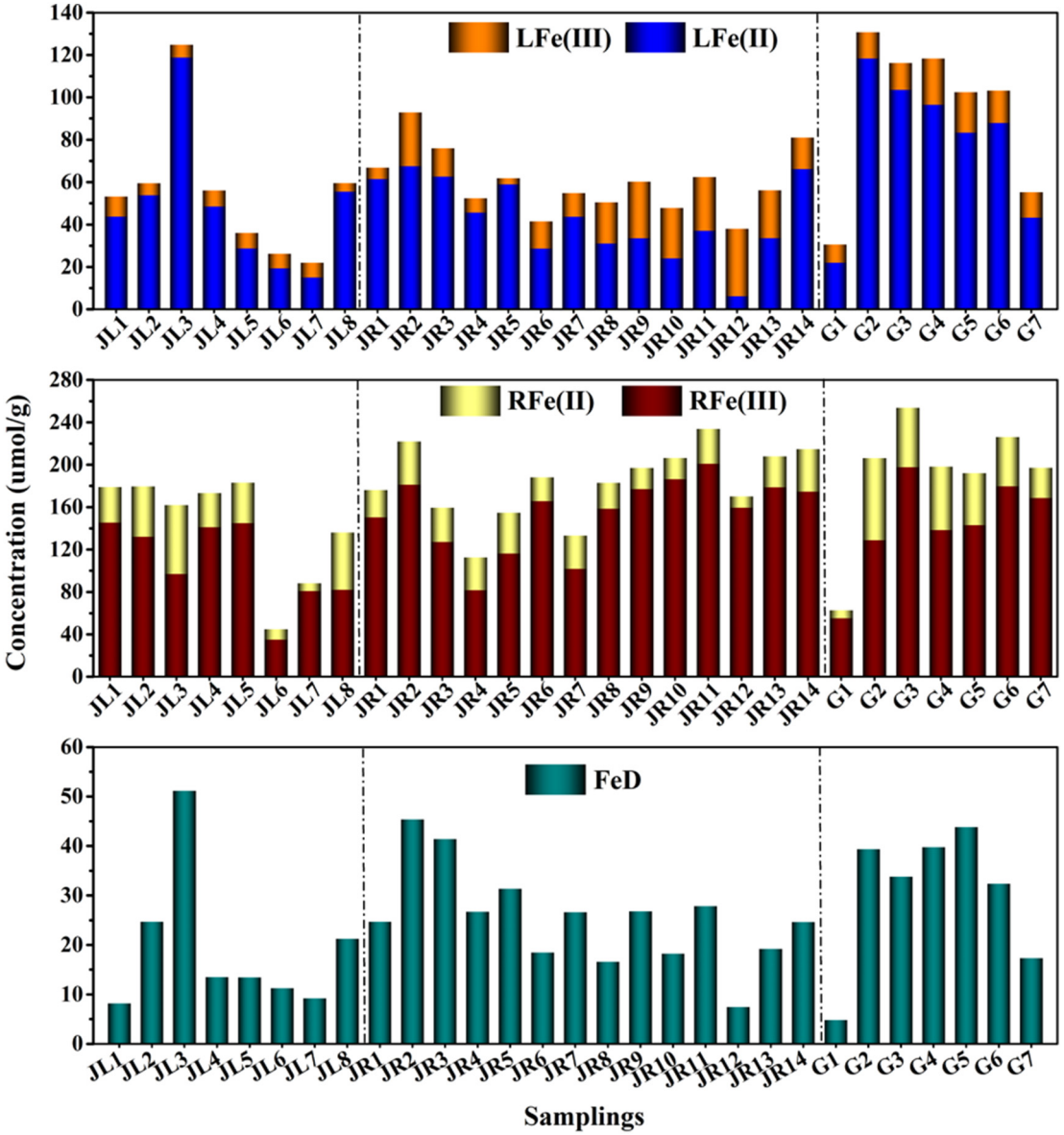

Fig. 4. Spatial distribution of solid phase Fe in surface sediments (a, LFe; b, RFe; c, FeD).

decrease C/N ratios by OM degradation (Nasir et al., 2016), which was confirmed by the high HAS and DOP in JR (Fig. 5 and Table S2).

4.2. Factors controlling S speciation

4.2.1. Iron sulfurization and pyritization

The values of AVS/CRS ratios, DOP and DOS are typically used to ascertain factors controlling the formation of AVS, CRS and the conversion of AVS to CRS (Gagnon et al., 1995). In this study, the AVS/CRS ratios in JL (mean 2.29 ± 0.17) and GD (mean 1.18 ± 0.08) were higher than 1, which were close to the ratios in adjacent coastal rivers in Laizhou Bay (mean 1.27, Sheng et al., 2015) and saltmarsh wetlands (mean 1) along coast of the North Yellow Sea (Yang et al., 2020), indicating low conversion from AVS to CRS occurred in study area. This notion was confirmed by low DOP and high DOS values in JL (DOP, 0.13 ± 0.02; DOS, 0.68 ± 0.05) and GD (DOP, 0.39 ± 0.03; DOS, 1.34 ± 0.13). This observation indicated that the sulfurization process occurred easily in JL and GD (Couture et al., 2016). In addition, RFe cannot limit Fe sulfide formation, but that the conversion of AVS to CRS was inhibited by AVS precipitation (Sun et al., 2016; Jørgensen et al., 2019). This phenomenon could be explained by the enrichment in RFe(III) in JL and GD as demonstrated by Eq. (6) (Oueslati et al., 2018). Conversely, in JR (Fig. 5b), a high portion of CRS (70% of RIS) and low AVS/CRS ratio (0.78) indicated that AVS was capable of rapid conversion to CRS (Meng et al., 2019) in contrast to JL and GD. This notion was supported by high DOP (up to 0.73) and DOS (up to 0.88) in JR. The different conversion efficiencies of AVS to CRS in three rivers were related to the redox conditions and/or sedimentation rates (Couture et al., 2016; Qin et al., 2019).

The low TOC (0.25 ± 0.01%) and high DO (7.9 ± 0.02 mg/L) and ORP (259.5 ± 0.01 mV) in JL (Table S1) suggested that the top layers of surface sediment were aerobic; these conditions would inhibit sulfate reduction and enhance S—Fe oxidation (Brocławik et al., 2020; Yang et al., 2020). This finding was consistent with low RIS retention fractions in JL (15.2% of total S). Because temporary aerobic conditions followed the brine (with high salinity) input from the salt fields (especially at JL4 and JL5), which increased Fe-oxide bioavailability (RFe(III) accounted for 75% of RFe). Therefore, rapid input and/or enrichment of Fe oxides in JL would result in the domination of dissimilatory Fe reduction rather than sulfate reduction (Eqs. (9) and (10)) (van de Velde

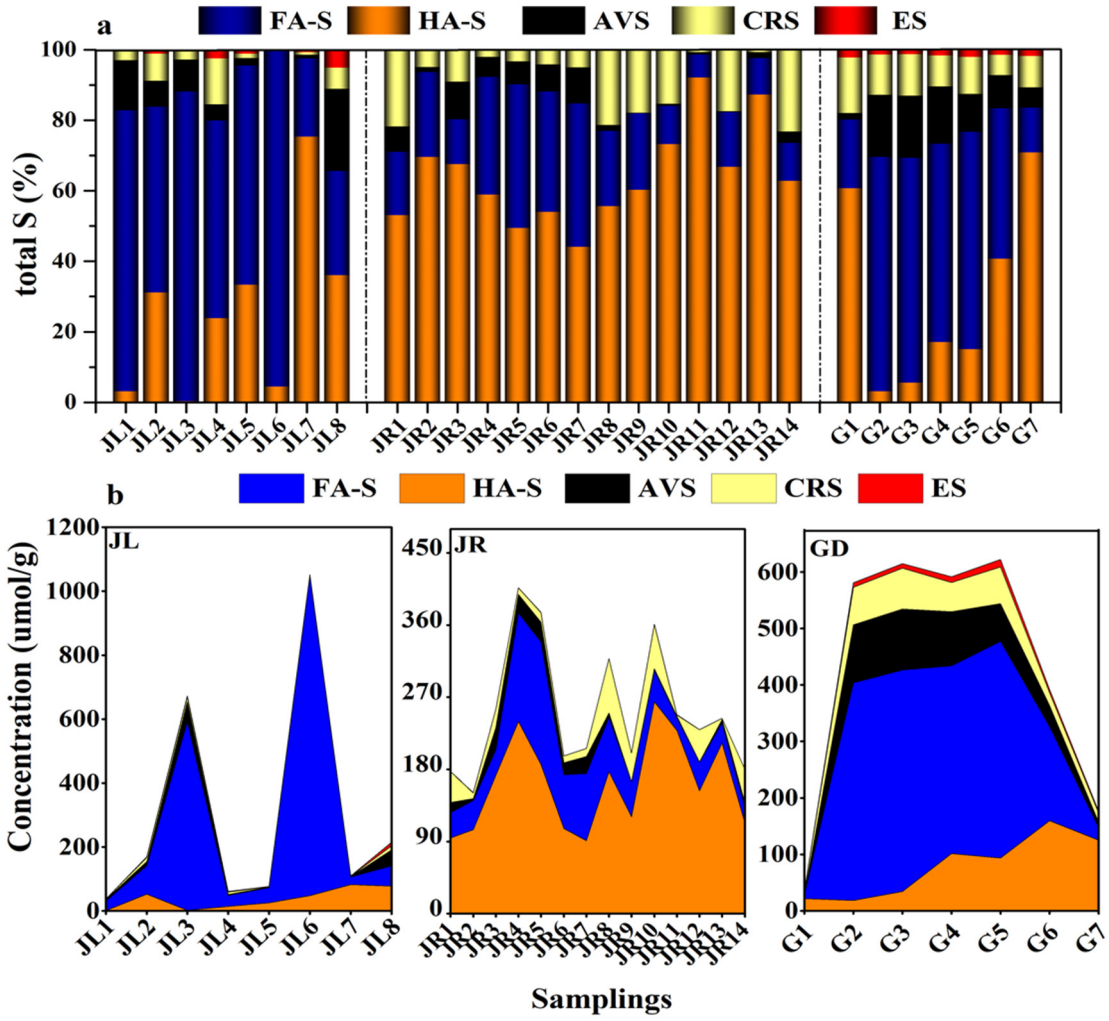

Fig. 5. Proportions (a) and concentrations (b) of different S fractions in surface sediments.

et al., 2018; Yang et al., 2020). However, the sediments often become anoxic due to stratification by halocline under high salinity, which allows H_2S to diffuse into surface sediments or above the sediment-water interface by the dissimilatory reduction of sulfate (Riedinger et al., 2017; Zhao et al., 2019). Moreover, the sulfate-reducing reaction at low pH in JL (low as 2.79) would be insufficient since adequate H^+ would inhibit the solubility of polysulfide (Eq. (11)) (Giuffrè and Vicente, 2018). These processes subsequently greatly favored the accumulation of AVS in relation to that of the CRS formation. The AVS dominated the RIS in JL, which confirmed the above hypothesis.

$$Fe^{2+} + 1/4O_2 + 3/2H_2O \rightarrow 2H^+ + FeOOH \quad (9)$$

$$4FeOOH + 1/2\ H_2S + 7H^+ \rightarrow 4Fe^{2+} + 1/2{SO_4}^{2-} + 6H_2O \quad (10)$$

$$S^0 + H_2O + 3/2O_2 \rightarrow 2H^+ + {SO_4}^{2-} \quad (11)$$

A previous study reported that higher AVS/CRS ratios are typically observed in rapidly deposited sediments (Gagnon et al., 1995). In slowly accumulating sediments, AVS is a minor component of the RIS or even absent when CRS accumulates rapidly (Yang et al., 2020). Accordingly, the high ratio in GD could result from a rapid sediment accumulation rate related to the increased incidence of reducing conditions and bottom water hypoxia/anoxia by the process of OM decomposition (Kraal et al., 2013; van de Velde et al., 2018). Therefore, the combination of strong sulfate reduction and weak sulfide oxidation in GD sediments could lead to the stabilization of the RIS pool as AVS (Morgan et al., 2012; Shi et al., 2019). Abundant RFe(II) was noted in JL (35.94 ± 8.78 μmol/g) and GD (46.44 ± 3.64 μmol/g), but levels were low in JR (28.52 ± 2.66 μmol/g). Therefore, excessive RFe(II) could inhibit the accumulation of reduced S (HS^- and H_2S) in the porewater in JL and GD due to AVS precipitation (Eq. (12)) (Liu et al., 2014). Thus, the weak diffusion of H_2S towards the redox boundary combined with high sedimentation rates restricted the solubility of solid ES (Eq. (11)), which could otherwise form polysulfide (Eq. (2)) (Zhang et al., 2018). This hypothesis was confirmed by higher ES retention efficiencies in JL and GD compared to JR (Fig. 5). The formation of polysulfides would subsequently activate the pyritization process (Eq. (13)) and thereby increase the conversion rate of AVS to CRS (Jørgensen et al., 2019), thus explaining the low AVS/CRS ratio in JR.

$$Fe^{3+} + HS^- \rightarrow 2Fe^{2+} + S^0 + H^+ \quad (12)$$

$${S_n}^{2-} + FeS \rightarrow FeS_2 + {S^{2-}}_{n-1} \quad (13)$$

4.2.2. Transformation of OS in sediments

Geochemistry processes always play crucial roles in controlling the transformation of sedimentary OS, particularly during early diagenesis (Morgan et al., 2012; Kraal et al., 2013). Sedimentary FAS dominated the total S pool in JL and GD, far exceeding FAS in JR, which was attributed to the trophic status of the environment (Fakhraee and Katsev,

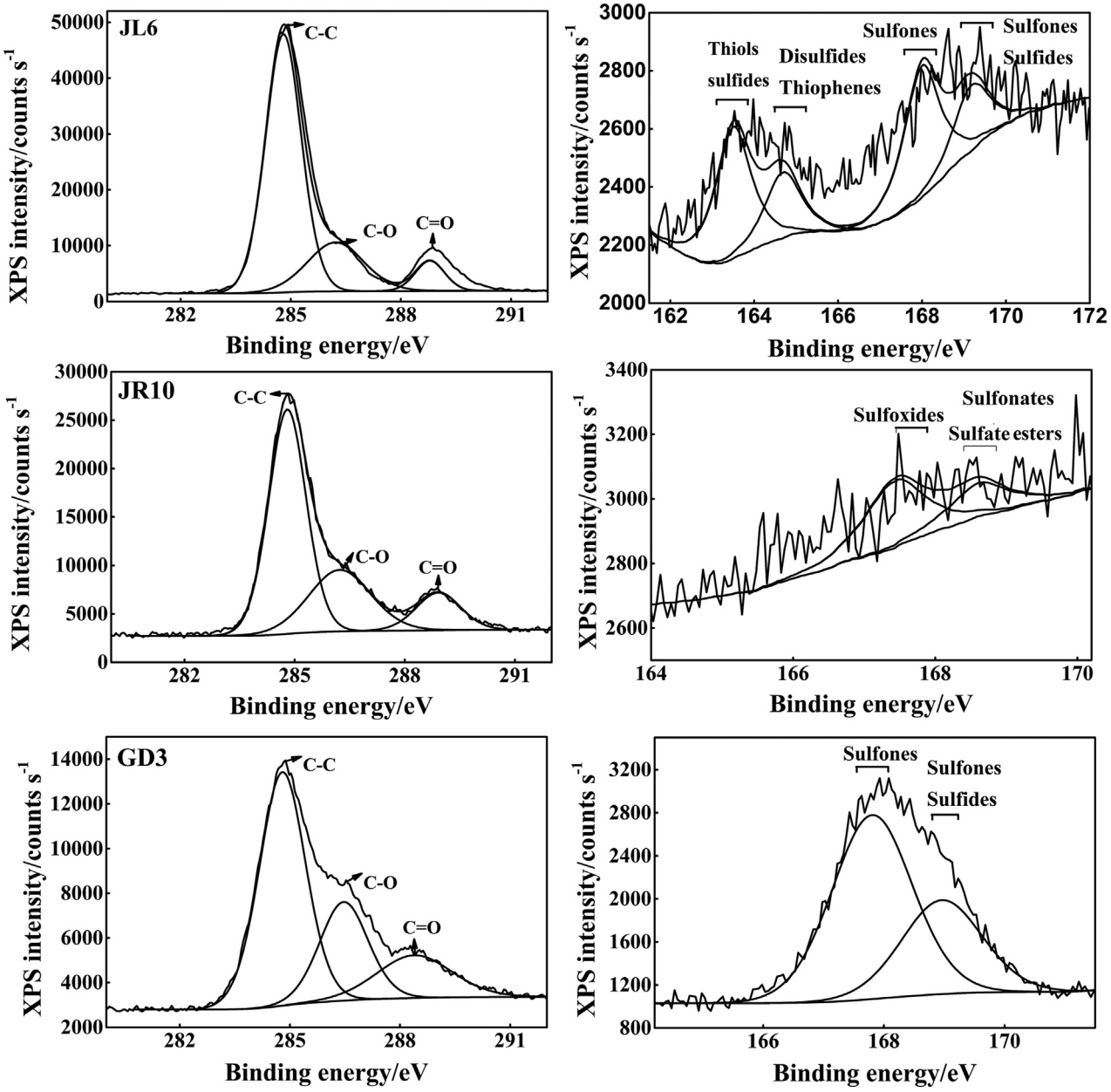

Fig. 6. Typical spectral simulation of C1s and S2p photopeaks observed in XPS spectrum.

Table 1
The XPS S2p analysis of surface sediments.

Sampling sites	Binding energies (eV)	Model compound	Area (%)
JL6	163.5	Thiols sulfides	33
	164.7	Disulfides thiophenes	17
	168.0	Sulfones	33
	169.1	Sulfate	17
JR10	167.4	Sulfoxides	67
	168.6	Sulfonates and Sulfate esters	33
GD3	167.8	Sulfones	66
	169.0	Sulfate	34

2019). Generally, high FAS exists in eutrophic environments because FA is more readily sulfurized during diagenesis compared with HA at the redox boundary (Brüchert, 1998; Zhu et al., 2014). This notion was confirmed by high levels of FAS (approximately 5 times greater than HAS) and DOS (JL, 0.68; GD, 1.34) in JL and GD (Fig. 5 and Table S2), which was much higher than previous observations in eutrophic Jiaozhou Bay (7.9–70 μmol/g, Zhu et al., 2014; Chen et al., 2014). This phenomenon suggested that high FAS was closely associated with allochthonous (terrestrial production) input from terrestrial point and non-point source pollution (Shi et al., 2019; Wang et al., 2020) because allochthonous sources contain substantial amounts of RFe oxides and OM (Fig. 4 and Table S1). Thus, the rapid input or enrichment of Fe oxides plus frequent redox oscillations in surface sediments promote sulfurization through rapid generation of intermediate S species *via* partial oxidation of sulfides by RFe oxides (Wang et al., 2016; Riedinger et al., 2017; Zhang et al., 2018). These intermediates could be formed during the reaction between OM and dissolved sulfide, presenting H_2S accumulation in FA (Brüchert, 1998; Einsiedl et al., 2008). This process would be regulated by the radical addition reaction of H_2S to quinones and by the formation of aryl thio-compounds (Giuffrè and Vicente, 2018). Additionally, high OM enrichment in surface sediments (especially in GD) was also favorable to sulfurization. Excessive sulfide produced *via* bacterial sulfate reduction may mitigate or even eliminate competitive

inhibition of Fe sulfide formation (Chen et al., 2014; Zhang et al., 2020). The distribution of RIS forms (summarized in Table S3) and XPS data (Table 1) also showed that reduced S compounds constituted a significantly higher proportion of S in GD compared to JL and JR. Accordingly, the availability of RFe and OM are important factors that control FAS formation, which clearly demonstrates the anthropogenic impacts on benthic geochemistry in the coastal river sediments.

In undefiled JR, high HAS and low FAS are probably related to HA and intrinsically refractory during early diagenesis (Zhu et al., 2013). This notion was supported by XPS results, which demonstrated that the OS was stored as stable compounds of sulfonates and ester-sulfates (Fig. 6). This finding was also consistent with a study by Morgan et al. (2012), suggesting HAS were likely associated with organic structures (such as macromolecules) in the sediment. Previous studies have confirmed that ester-sulfates can be formed *via* biotic rather than abiotic mechanisms (Fakhraee and Katsev, 2019; Jørgensen et al., 2019; Brocławik et al., 2020). Regarding the formation of sulfonates, both geochemical and biological pathways are possible (Zhu et al., 2014; Fakhraee et al., 2019). Biosynthetic HAS is derived from aquatic vascular plants or from dissolved sulfate assimilated by algae (Giordano and Raven, 2014). Since the roots of aquatic vascular plants extend into anoxic sediments, dissolved sulfide can be assimilated either directly or *via* reoxidation to sulfate (Yang et al., 2020). This notion was further supported by the fact that the sedimentary environment in JR was characterized by oxidizing-to-reducing oscillation since abundant aquatic organisms are reflected by low C/N ratios (<10). Such conditions changed the residence time of RIS species in the vicinity of the interface, and more sulfides were further oxidized into intermediate S (Sun et al., 2016; Couture et al., 2016). Moreover, rapid inputs and/or enrichments of RFe could also be used as oxidizing agents to oxidize H_2S in porewater, improving the production of intermediate S (Giuffrè and Vicente, 2018; Ma et al., 2019). During this process, a portion of sulfur-containing molecules or released free sulfide quickly reacts with reactive sites on adjacent biomolecules (Oueslati et al., 2018; Fakhraee et al., 2019). Cross-linking of HA with organic molecules contributed to the increase in the content of macromolecular organic polymers during diagenesis (Morgan et al., 2012; Fakhraee et al., 2017), resulting in the accumulation of HAS in JR.

The sulfur-bearing OM deposited in riverine surface sediment mainly originates from allochthonous terrestrial sources and autochthonous primary production, where it typically dominates the total S pool (Zhu et al., 2013; Couture et al., 2016). Sedimentary OM predominantly contains oxidized OS (R-O-SO_3-H groups, such as ester-sulfates, sulfoxides/sulfone) or reduced OS (R-SH groups, such as thiols and sulfide) (Couture et al., 2016; Fakhraee et al., 2017). In both pools (endogenous and exogenous sources), R-O-SO_3-H appears to be the dominant species. In this work, high levels of R-O-SO_3-H groups are consistent with the above findings (Fig. 6 and Table 1), suggesting that highly oxidized OS is stored in surface sediments. Thus, allochthonous terrestrial sources and autochthonous primary production contained large amounts of reactive OM (Giordano and Raven, 2014), and aquatic life can break it down further, producing reactively reduced OS compounds (*e.g.*, thiols) and RIS in anoxic sediments, such as in JL and GD. R-SH could be rapidly oxidized to form sulfoxides/sulfone and then subsequently form stable compounds of sulfonates, which may resist remineralization (Ferdelman et al., 1991). Moreover, OS could also be utilized by microorganisms, such as bacteria that cleave the bonds in R-O-SO_3-H (*e.g.*, aryl sulfatase) and R-SH (*e.g.*, cysteine lyase), releasing SO_4^{2-} and HS^-, respectively, to sediment porewater (Fakhraee et al., 2017). In the aerobic sediment, RIS can be oxidized to provide an additional source of sulfate for anaerobic microbial oxidation of sedimentary OM (Wang et al., 2016; Yang et al., 2020). Therefore, sulfate reduction may dominate dissimilatory Fe reduction by the coupled dynamics between the RIS and OS cycles, accumulating as reduced S species of R-SH and RIS in the anoxic sediment. These OS transformations would lead to low turnover rates of the total OS pool and therefore enhance OS accumulation, resulting in high OS in surface sediments in coastal rivers.

4.3. Rapid sulfide-buffering capacity

Rapid sulfide-buffering capacities (β_L) represents a potential buffering capability for the removal of dissolved sulfide by reaction with Fe (Heijs et al., 1999; Azzoni et al., 2005). In this work, calculated β_L values ranged from 11.6 to 66.5 μmol/g in JL (average 40.9), 32.8 to 103.3 μmol/g in JR (average 58.3) and 14.7 to 74.1 μmol/g in GD (average 41). In comparison, Table 2 showed the β_L and some relevant parameters together with other sediments impacted by anthropogenic perturbations. The values of β_L for three rivers were roughly similar to Fe-rich sediments of intertidal mudflat (Meng et al., 2019) but substantially increased compared with Fe-poor sediments in Arcachon Bay (Heijs et al., 1999) and coastal lagoons (Signorini et al., 2008), indicating that the high LFe played a critical role in the rapid buffering of dissolved sulfide. The AVS/LFe ratio can be used as an indicator for buffering saturation of Fe towards free sulfide (fraction of LFe has been sulfurized) (Azzoni et al., 2005). An AVS/LFe ratio < 0.25 indicates a state of high residual buffering capacity, and a value between 0.75 and 1 indicates exhausted buffering capacity. The activity of sulfide produced by bacterial sulfate reduction is expected to be released when AVS/LFe is greater than 1. In this work, the ratios of AVS/LFe in GD were 0.02–0.93 (mean 0.53), which were close to the range in coastal lagoon sediments (0.05–0.84, Signorini et al., 2008), suggesting buffering saturation in surface sediments. This finding implied that β_L appeared to be exhausted in surface sediments in GD, where sulfate reduction rates (SRR) were probably high due to the impact of pollution as reflected by high TOC enriched in surface sediments (Table S1). In JR sediments, AVS/LFe was less than 0.5, indicating excess buffering capacity of LFe for sulfide production. However, in JL sediments, AVS/LFe values were <0.25 except for JL3 (0.5) and JL8 (0.84). This result is similar to that observed in other studies (Zhu et al., 2012; Liu et al., 2014), suggesting a high residual buffering capacity at most sites. This phenomenon was probably related to the effects of frequent artificial disturbance (such as dredging and sand excavation) with sediment porosity (coarse sediments), which would make free sulfide stripping by the N_2 gas stream easier (Oueslati et al., 2018). Moreover, the removal of free sulfide might stimulate SRR (Qin et al., 2019; Ma et al., 2019). Therefore, free sulfide accumulated in only several sites in JL and most sites in GD, increasing the threat of benthic S poisoning. Correspondingly, most sites in JR and JL experienced high buffering saturation, which does not cause detrimental effects on benthic ecosystems, such as Jiaozhou Bay and East China Sea inner shelf sediments (Zhu et al., 2012; Liu et al., 2014).

Table 2
The comparison of buffering capacities and relevant parameters at various areas.

Location	Site	LFe (μmol/g)	β_L (μmol/g)	AVS/LFe	Source
Arcachon Bay	A	3.4–20	−2.1-24	0.02–1.9	Heijs et al., 1999
	B	47–80	31-59	0.28–0.36	
Coastal lagoons	Caprolace	14.7–37.7	3.4–26.3	0.35–0.84	Signorini et al., 2008
	Fogliano	35–55.9	15.9–44.7	0.05–0.72	
Jiaozhou Bay	J1	106–148	108–142	0.0005–0.10	Zhu et al., 2013
	J2	71.4–99	82–98	0.001–0.007	
	J3	73–85	75–94	0.002–0.007	
East China sea	C	65–150	73–167	0–0.04	Liu et al., 2014
Jiaolai River	JL	22–125	12–67	0.05–0.84	
Jiahe River	JR	38–93	33–103	0.01–0.44	This study
Guangdang River	GD	31–131	15–74	0.02–0.93	

5. Conclusions

The environmental transformations of S in coastal river sediments provide evidence for a link between RIS formation and OS sulfurization. OS dominated total S and correlated with the availability of OM and RFe. Terrigenous inputs and sulfurization may be important factors determining the high enrichment of FAS through the reduction of S. Autochthonous biological inputs were potential sources HAS from S oxidization. The main sources of S in surface sediments were deposited in the form of R-O-SO_3-H. Aquatic life can break it down further, and reduced S compounds accumulated as R-SH and RIS in anoxic sediments. The generation and accumulation of RIS in coastal rivers are regulated by TOC and RFe in sedimentary environments, where AVS and CRS dominated RIS. RFe oxides are the major controlling factors of conversation from H_2S to AVS, while the ES is the major controlling factor of conversion from AVS into CRS. The transformations between OS and RIS would lead to low turnover rates of the total OS pool and therefore would enhance OS accumulation in coastal rivers.

CRediT authorship contribution statement

All authors have contributed to the manuscript. Ming Jiang wrote and prepared the figures and tables of the manuscript. All authors revised and approved the final manuscript.

Declaration of competing interest

The authors declare that they have no known competing financial interests or personal relationships that could have appeared to influence the work reported in this paper.

Acknowledgment

This work was partially supported by the Strategic Priority Research Program of the Chinese Academy of Sciences (Grant No.: XDA23050203) and the National Natural Science Foundation of China (Grant No: 41373100). Additional support was from the Key Project of Research and Development Plan of Yantai (Grant No: 2018ZHGY080) and the Key Research and Development Program of Shandong Province (Grant No. 2019GSF109002).

Appendix A. Supplementary data

Supplementary data to this article can be found online at https://doi.org/10.1016/j.scitotenv.2020.141829.

References

Azzoni, R., Giordani, G., Viaroli, P., 2005. Iron–sulphur–phosphorus interactions: implications for sediment buffering capacity in a Mediterranean eutrophic lagoon (Sacca di Goro, Italy). Hydrobiologia 550 (1), 131–148. https://doi.org/10.1007/S10750-005-4369-X.

Bao, L., Li, X., Su, J., 2020. Alteration in the potential of sediment phosphorus release along series of rubber dams in a typical urban landscape river. Sci. Rep. 10 (1), 2714. https://doi.org/10.1038/S41598-020-59493-3.

Berner, R.A., Scott, M.R., Thomlinson, C., 1970. Carbonate alkalinity in the pore water of anoxic marine sediments. Limnol. Oceanogr. 15, 544–549. https://doi.org/10.4319/lo.1970.15.4.0544.

Brocławik, O., Łukawska-Matuszewska, K., Brodecka-Goluch, A., Bolałek, J., 2020. Impact of methane occurrence on iron speciation in the sediments of the Gdansk Basin (Southern Baltic Sea). Sci. Total Environ. 721, 137718. https://doi.org/10.1016/J.SCITOTENV.2020.137718.

Brüchert, V., 1998. Early diagenesis of sulfur in estuarine sediments: the role of sedimentary humic and fulvic acids. Geochim. Cosmochim. Acta. 62 (9), 1567–1586. https://doi.org/10.1016/S0016-7037(98)00089-1.

Canfield, 1989. Reactive iron in marine sediments. Geochim. Cosmochim. Acta. 53 (3), 619–632. https://doi.org/10.1016/0016-7037(89)90005-7.

Chen, K.K., Zhu, M.X., Yang, G.P., Fan, D.J., Huang, X.L., 2014. Spatial distribution of organic and pyritic sulfur in surface sediments of eutrophic Jiaozhou Bay, China: clues to anthropogenic impacts. Mar. Pollut. Bull. 88 (1), 284–291. https://doi.org/10.1016/J.MARPOLBUL.2014.08.029.

Couture, R.M., Fischer, R., Cappellen, P.V., Gobeil, C., 2016. Non-steady state diagenesis of organic and inorganic sulfur in lake sediments. Geochim. Cosmochim. Acta 194, 15–33. https://doi.org/10.1016/J.GCA.2016.08.029.

Einsiedl, F., Mayer, B., Schäfer, T., 2008. Evidence for incorporation of H_2S in groundwater fulvic acids from stable isotope ratios and sulfur K-edge X-ray absorption near edge structure spectroscopy. Environ. Sci. Technol. 42 (7), 2439–2444. https://doi.org/10.1021/ES7025455.

Fakhraee, M., Katsev, S., 2019. Organic sulfur was integral to the Archean sulfur cycle. Nat. Commun. 10 (1), 4556. https://doi.org/10.1038/S41467-019-12396-Y.

Fakhraee, M., Li, J., Katsev, S., 2017. Significant role of organic sulfur in supporting sedimentary sulfate reduction in low-sulfate environments. Geochim. Cosmochim. Acta 213, 502–516. https://doi.org/10.1016/j.gca.2017.07.021.

Ferdelman, T.G., Church, T.M., Luther, G.W., 1991. Sulfur enrichment of humic substances in a Delaware salt marsh sediment core. Geochim. Cosmochim. Acta 55 (4), 979–988. https://doi.org/10.1016/0016-7037(91)90156-Y.

Gagnon, C., Mucci, A., Pelletier, É., 1995. Anomalous accumulation of acid-volatile sulphides (AVS) in a coastal marine sediment, Saguenay Fjord, Canada. Geochim. Cosmochim. Acta 59 (13), 2663–2675. https://doi.org/10.1016/0016-7037(95)00163-T.

Giordano, M., Raven, J.A., 2014. Nitrogen and sulfur assimilation in plants and algae. Aquat. Bot. 118, 45–61. https://doi.org/10.1016/j.aquabot.2014.06.012.

Giuffrè, A., Vicente, J.B., 2018. Hydrogen sulfide biochemistry and interplay with other gaseous mediators in mammalian physiology. Oxidative Med. Cell. Longev. 2018 (2018), 6290931. https://doi.org/10.1155/2018/6290931.

Heijs, S.K., Jonkers, H.M., Gemerden, H. van, Schaub, B.E.M., Stal, L.J., 1999. The buffering capacity towards free sulphide in sediments of a coastal lagoon (Bassin d'Arcachon, France) - the relative importance of chemical and biological processes. Estuar. Coast. Shelf Sci. 49 (1), 21–35. https://doi.org/10.1006/ECSS.1999.0482.

Jørgensen, B.B., Findlay, A.J., Pellerin, A., 2019. The biogeochemical sulfur cycle of marine sediments. Front. Microbiol. 10, 849. https://doi.org/10.3389/FMICB.2019.00849.

Kraal, P., Burton, E.D., Bush, R.T., 2013. Iron monosulfide accumulation and pyrite formation in eutrophic estuarine sediments. Geochim. Cosmochim. Acta. 122, 75–88. https://doi.org/10.1016/J.GCA.2013.08.013.

Li, Z., Sheng, Y., Shi, W., Sun, Q., Mortimer, R.J.G., 2016. Influence of salinity on COD measurements in coastal water management. Desalin. Water Treat. 57 (39), 18338–18345. https://doi.org/10.1080/19443994.2015.1091996.

Liu, J., Zhu, M.-X., Yang, G.-P., Shi, X.-N., Yang, R.-J., 2014. Quick sulfide buffering in inner shelf sediments of the East China Sea impacted by eutrophication. Environ. Earth Sci. 71 (1), 465–473. https://doi.org/10.1007/S12665-013-2454-4.

Liu, Q., Sheng, Y., Jiang, M., Zhao, G., Li, C., 2020. Attempt of basin-scale sediment quality standard establishment for heavy metals in coastal rivers. Chemosphere 245, 125596. https://doi.org/10.1016/J.CHEMOSPHERE.2019.125596.

Ma, W.W., Zhu, M.X., Yang, G.P., Li, W.J., Meng, T., Li, T., 2019. Diagenesis of sulfur, iron and phosphorus in sediments of an urban bay impacted by multiple anthropogenic perturbations. Mar. Pollut. Bull. 146, 366–376. https://doi.org/10.1016/J.MARPOLBUL.2019.06.081.

Meng, T., Zhu, M.X., Ma, W.W., Gan, Z.X., 2019. Sulfur, iron, and phosphorus geochemistry in an intertidal mudflat impacted by shellfish aquaculture. Environ. Sci. Pollut. 26 (7), 6460–6471. https://doi.org/10.1007/S11356-018-04114-W.

Meyers, P.A., 1997. Organic geochemical proxies of paleoceanographic, paleolimnologic, and paleoclimatic processes. Org. Geochem. 27 (5), 213–250. https://doi.org/10.1016/S0146-6380(97)00049-1.

Morgan, B., Burton, E.D., Rate, A.W., 2012. Iron monosulfide enrichment and the presence of organosulfur in eutrophic estuarine sediments. Chem. Geol. 296, 119–130. https://doi.org/10.1016/J.CHEMGEO.2011.12.005.

Mott, R.A., Wilkinson, H.C., 2007. The use of the Eschka method for the determination of high sulphur contents. J. Chem. Technol. Biotechnol. 3 (5), 218–223. https://doi.org/10.1002/JCTB.5010030506.

Nasir, A., Lukman, M., Tuwo, A., Hatta, M., Tambaru, R., Nurfadilah, 2016. The use of C/N ratio in assessing the influence of land-based material in coastal water of South Sulawesi and Spermonde Archipelago, Indonesia. Front. Mar. Sci. (3), 266 https://doi.org/10.3389/FMARS.2016.00266.

Oueslati, W., Helali, M.A., Zaaboub, N., Sebei, A., Added, A., Aleya, L., 2018. Sulfide influence on metal behavior in a polluted southern Mediterranean lagoon: implications for management. Environ. Sci. Pollut. Res. 25 (3), 2248–2264. https://doi.org/10.1007/S11356-017-0529-6.

Qin, S.S., Zhu, M.X., Yang, G.P., Wang, D., 2019. Atypical diagenesis of sulfur and iron in sediments of the river-dominated Bohai Sea (China). J. Mar. Syst. 189, 116–126. https://doi.org/10.1016/J.JMARSYS.2018.10.004.

Riedinger, N., Brunner, B., Krastel, S., Arnold, G.L., Wehrmann, L.M., Formolo, M.J., ... Kasten, S., 2017. Sulfur Cycling in an iron Oxide-Dominated, Dynamic Marine Depositional System: The Argentine Continental Margin. Frontiers in Earth Science 5, 33. https://doi.org/10.3389/FEART.2017.00033.

Sheng, Y., Sun, Q., Shi, W., Bottrell, S., Mortimer, R., 2015. Geochemistry of reduced inorganic sulfur, reactive iron, and organic carbon in fluvial and marine surface sediment in the Laizhou Bay region, China. Environ. Earth Sci. 74 (2), 1151–1160. https://doi.org/10.1007/S12665-015-4101-8.

Shi, J., Zhang, B., Qiu, R., Lai, C., Jiang, Y., He, C., Guo, J., 2019. Microbial chromate reduction coupled to anaerobic oxidation of elemental sulfur or zerovalent iron. Environ. Sci. Technol. 53 (6), 3198–3207. https://doi.org/10.1021/ACS.EST.8B05053.

Signorini, A., Massini, G., Migliore, G., Tosoni, M., Varrone, C., Izzo, G., 2008. Sediment biogeochemical differences in two pristine Mediterranean coastal lagoons (in Italy) characterized by different phanerogam dominance-a comparative approach. Aquat. Conserv. Mar. Freshwat. Ecosyst. 18 (S1), S27–S44. https://doi.org/10.1002/AQC.953.

Sun, Q., Sheng, Y., Yang, J., Bonito, M.D., Mortimer, R.J.G., 2016. Dynamic characteristics of sulfur, iron and phosphorus in coastal polluted sediments, north China. Environ. Pollut. 219, 588–595. https://doi.org/10.1016/J.ENVPOL.2016.06.019.

van de Velde, S., Van Lancker, V., Hidalgo-Martinez, S., Berelson, W.M., Meysman, F.J.R., 2018. Anthropogenic disturbance keeps the coastal seafloor biogeochemistry in a transient state. Sci. Rep. 8 (1), 5582. https://doi.org/10.1038/s41598-018-23925-y.

Wang, Y., Zhu, L., Wang, J., Ju, J., Lin, X., 2012. The spatial distribution and sedimentary processes of organic matter in surface sediments of Nam Co, Central Tibetan Plateau. Chin. Sci. Bull. 57 (36), 4753–4764. https://doi.org/10.1007/S11434-012-5500-9.

Wang, J., Chen, J., Dai, Z., Yang, H., Ma, C., 2016. Sulfur speciation in the surface sediments of lakes from different regions, China: characterization by S K-edge XANES spectroscopy. J. Chem. 2016, 1–9. https://doi.org/10.1155/2016/3672348.

Wang, S., Zhang, B., Li, T., Li, Z., Fu, J., 2020. Soil vanadium(V)-reducing related bacteria drive community response to vanadium pollution from a smelting plant over multiple gradients. Environ. Int. 138, 105630. https://doi.org/10.1016/J.ENVINT.2020.105630.

Yang, S., Tang, M., Yim, W.W.-S., Zong, Y., Huang, G., Switzer, A.D., Saito, Y., 2011. Burial of organic carbon in Holocene sediments of the Zhujiang (Pearl River) and Changjiang (Yangtze River) estuaries. Mar. Chem. 123 (1), 1–10. https://doi.org/10.1016/J.MARCHEM.2010.07.001.

Yang, J., Paytan, A., Yang, Y., Wei, S., Liu, B., Cui, H., ... Zhao, Y., 2020. Organic carbon and reduced inorganic sulfur accumulation in subtropical saltmarsh sediments along a dynamic coast, Yancheng, China. Journal of Marine Systems, 103415 https://doi.org/10.1016/j.jmarsys.2020.103415.

Zhang, B., Qiu, R., Lu, L., Chen, X., He, C., Lu, J., Ren, Z.J., 2018. Autotrophic vanadium (V) bioreduction in groundwater by elemental sulfur and zerovalent iron. Environ. Sci. Technol. 52 (13), 7434–7442. https://doi.org/10.1021/ACS.EST.8B01317.

Zhang, B., Wang, Z., Shi, J., Dong, H., 2020. Sulfur-based mixotrophic bio-reduction for efficient removal of chromium (VI) in groundwater. Geochim. Cosmochim. Acta 268, 296–309. https://doi.org/10.1016/J.GCA.2019.10.011.

Zhao, G., Sheng, Y., Jiang, M., Zhou, H., Zhang, H., 2019. The biogeochemical characteristics of phosphorus in coastal sediments under high salinity and dredging conditions. Chemosphere 215, 681–692. https://doi.org/10.1016/j.chemosphere.2018.10.015.

Zhu, M.X., Liu, J., Yang, G.P., Li, T., Yang, R.J., 2012. Reactive iron and its buffering capacity towards dissolved sulfide in sediments of Jiaozhou Bay, China. Mar. Environ. Res. 80, 46–55. https://doi.org/10.1016/J.MARENVRES.2012.06.010.

Zhu, M.X., Huang, X.L., Yang, G.P., Hao, X.C., 2013. Speciation and stable isotopic compositions of humic sulfur in mud sediment of the East China Sea: constraints on origins and pathways of organic sulfur formation. Org. Geochem. 63 (63), 64–72. https://doi.org/10.1016/J.ORGGEOCHEM.2013.08.003.

Zhu, M.X., Chen, Jih, L.J., Yang, G.P., Huang, X.L., Ma, C.Y., 2014. Humic sulfur in eutrophic bay sediments: characterization by sulfur stable isotopes and K-edge XANES spectroscopy. Estuar. Coast. Shelf Sci. 138 (138), 121–129. https://doi.org/10.1016/J.ECSS.2013.12.027.